Deformation behaviour of liquid crystal polymer fibres: 1. Converting spectroscopic data into mechanical stress–strain curves in tension and compression

C. Vlattas and C. Galiotis*
Department of Materials, Queen Mary & Westfield College, Mile End Road, London E1 4NS, UK
(Received 26 May 1993; revised 16 November 1993)

A modified version of the cantilever bending beam method is employed to subject a number of rigid and semi-rigid rod fibres to a gradient of axial compressive and tensile stresses. The molecular deformation of the filaments in tension and compression is monitored by scanning along the length of the filaments with a laser Raman microprobe. Strain hardening phenomena in tension and strain softening phenomena in compression are closely studied. Finally, a method for converting the Raman spectroscopic data into stress–strain curves in both tension and compression, is demonstrated.

(Keywords: fibres; Raman spectroscopy; deformation behaviour)

INTRODUCTION

The deformation of fibres spun from liquid-crystalline solutions has been the subject of numerous studies over the last 15 years in an attempt to understand and subsequently exploit the unique mechanical properties of these polymer fibres in composite applications. The tensile modulus of these fibres has been found to range between 80 GPa for a low modulus aramid fibre[1] and 370 GPa for a heat-treated poly(*p*-phenylene benzobisoxazole) (PBO) fibre[2], while the tensile strength of certain types of these fibres can be as high as 5 GPa[3]. With respect to their tensile properties, liquid crystal polymer (LCP) fibres represent a viable and potentially more economical alternative to carbon fibres for certain composite applications. However, it is well established that these fibres are an order of magnitude weaker in compression in spite of their superior elongational strength and stiffness. It is indeed ironic that the high anisotropy and the nematic liquid crystalline character of these fibres, which are the main causes of their superior tensile performance, are also held responsible for their instability in compression[4].

Although the molecular as well as the supramolecular response of LCP fibres to an applied tensile load is now well documented and satisfactory models have been developed to account for the non-linearity in tension, comparatively very little has been done towards understanding the molecular response of these fibres under the influence of an applied stress in compression. Generally the published work can be classified into two categories: (1) measurements of the critical compressive stress or strain to failure of these fibres; and (2) investigations into the mode of failure in compression.

The tests employed in the first category have been extensively discussed in an earlier publication[5]. It suffices to say here that tests such as the 'elastica loop test'[6–8], the 'embedded fibre method'[9–12], the 'recoil test'[13–15] and the 'bending beam method'[16], estimate a value of 'compressive strength' using assumptions about the loading condition and deformation process. The only attempt to measure directly the response of a fibre to a compressive stress has been reported by Macturk *et al.*[17] but it is doubtful whether this method can produce accurate values of stresses and strains in the fibre due to limitations in experimentation and the influence of severe end-effects[17]. Reported values for the compressive strength of these fibres normally vary between 200 MPa[15] and a maximum 700 MPa[8,12]. In most cases the compressive modulus is taken to be equal to the tensile modulus of the fibres, an assumption which has been shown to be invalid[5].

The morphology of failed fibres in compression has been studied by methods such as optical and electron microscopy in the papers listed in category (2). The characteristic mode of compressive failure for most known LCP fibres is the formation of kink bands. These kinks can be as wide as one fibre diameter and can extend to a maximum length of 2 μm[18,19]. Most authors consider the kink bands to be regions of shear deformation occurring along slip planes which are separated from the undeformed part of the sample by sharp localized bending of the macromolecules[18,19]. Indisputable evidence for the generation of deformation zones during compressive failure of rigid-rod fibres in which a great deal of plastic strain is 'frozen' or, in other words, for the compressive 'yielding' of such rigid structures, has been provided by Martin and Thomas[19] by means of high-resolution electron microscopy (HREM). Finally, one should mention that kink band formation unlike

* To whom correspondence should be addressed

0032-3861/94/11/2335–13

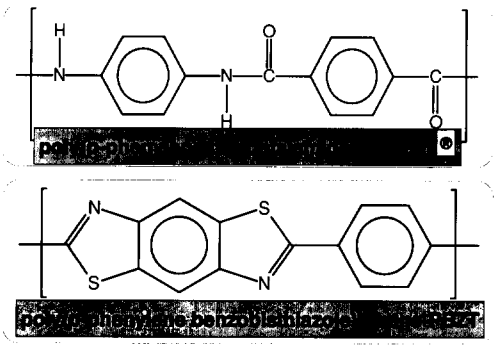

Figure 1 Chemical formulae of the LCP fibres studied in this work

shear fracture observed in high-modulus carbon fibres, absorbs considerable amounts of energy and therefore serves as a toughening mechanism in a number of military (bullet-proof jackets, helmets, etc.) or even medical (surgical gloves, etc.) composite applications.

In this study, a modified version of the cantilever bending beam method[20] is employed to subject a number of rigid and semi-rigid rod fibres to a gradient of axial compressive stress. For comparison purposes, side-by-side experiments were conducted on three grades of commercial Kevlar fibres (K29, K49 and K149), two grades of heat-treated Kevlar fibres of 1420 and 2120 denier, and a rigid-rod poly(*p*-phenylene benzobisthiazole) (PBZT) fibre. The chemical formulae of the fibres studied are given in *Figure 1*. The filaments were glued onto the bars by means of a thin acrylic film which, in turn, transmits the load to the fibres and supports them against global (Euler) instabilities. Provided that no slippage takes place between the fibre and the bar, the maximum strain on the surface of the bar varies linearly along the length of the beam and is only a function of the position on the bar, x, as determined by elastic beam theory[21]. The molecular deformation of the embedded fibres under axial compression is monitored by scanning along the length of the fibres with a laser Raman microprobe[5,20]. Past work has shown that Raman vibrational frequencies of the skeletal backbone shift to lower values under tension and to higher values under compression and well defined relationships between Raman frequency and applied stress or strain can be obtained for a whole range of polymeric or polymer-derived fibres[22].

In the first paper of this series[5], the Raman data in tension and compression were fitted at a first approximation with straight lines. Approximate estimates of the compression modulus were obtained by multiplying the tension modulus with a 'reduction' factor given by the ratio of the slopes of the Raman frequency shift *versus* strain in compression to that in tension[5]. Finally, rough estimates of the compression strength were obtained by multiplying the estimated compression modulus by the measured values of the strain required for fibre compression failure[5].

In this work, an improved methodology is presented which allows us to focus upon the deformation processes in tension as well as in compression using identical experimental conditions. The physical requirement for a smooth transition through the zero-strain point of the Raman frequency *versus* applied strain plot is obeyed. Thus, good estimates of the strain dependence of fibre modulus and of the compression strength are obtained.

EXPERIMENTAL

Specimen preparation

The polymer filaments were aligned on the top surface of poly(methyl methacrylate) (PMMA) bars. The free span, width and thickness of the bars were 50, 10 and 5 mm, respectively. The fibres were bonded onto the bars by spraying them with an acrylic (Krylon) spray. The thickness of the adhesive film was always kept to an optimum value of approximately one fibre diameter. The film was dried for several hours at room temperature under vacuum. Four different specimens of each type of fibre were tested. Full details of the preparation procedure are given in a previous publication[5].

Cantilever beam assembly

The cantilever beam configuration employed here and the formula used to derive the value of strain at the beam surface, are shown in *Figure 2*. The beam can be flexed up or down by means of a specially designed loading device, subjecting the fibre to compression or tension, respectively. The fibres under load were examined with a laser Raman microscope which was located above the flexed beam. Prior to cantilever compression testing, the Raman frequencies of all the embedded LCP fibres were recorded and all fibre specimens found to exhibit Raman frequency values different from the values of the stress-free fibre in the air were discarded. Furthermore, any fibres that contained residual stresses due to either film shrinkage and/or mishandling were not included in the measurements.

The possibility of slippage between fibre and the beam was examined using a four-point bend beam configuration where the strains are uniform between inner loading points. This study, which is presented in Appendix 1, showed that both configurations yield almost identical data for all fibres examined here.

Laser Raman spectroscopy

Raman spectra were taken with the 514.5 nm line of an argon ion laser. A modified Nikon microscope was used to focus the incident laser beam to a 2 μm spot on the fibre. Care was taken not to exceed a maximum laser power of 1 mW on the sample to avoid local overheating of the fibre/acrylic film system. The 180° backscattered light was collected by the microscope objective and focused on the entrance slit of a SPEX 1877 triple

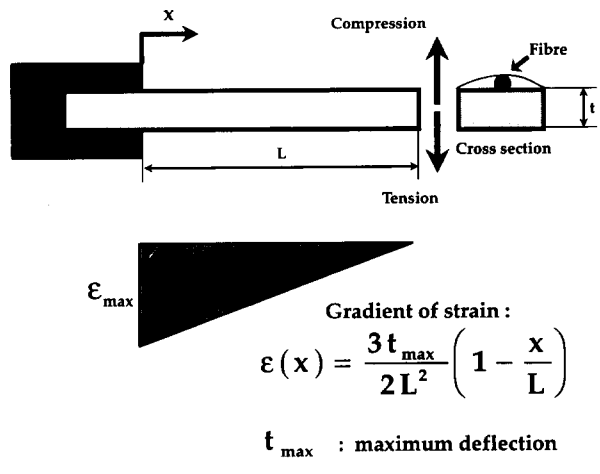

Figure 2 Schematic representation of the cantilever beam assembly

monochromator. A Wright Instruments charge coupled device (CCD), cooled by liquid nitrogen, was employed as a photon counting system for recording of the Raman spectra. All the Raman frequency values were derived by fitting Lorentzian routines to the CCD raw data.

Tensile testing

Single filaments were tested in tension according to the ASTM procedure[23] on a Hounsfield H25KM Universal Mechanical Tester using a 20 N load cell. The filaments were mounted across elliptical holes 25 mm in their long axis, which had been previously punched on rectangular paper tabs. The fibres were bonded to the paper tabs with Araldite adhesive and were subsequently gripped in the jaws of the microtester. The fibres were deformed at a strain rate of $0.04\,min^{-1}$ up to tensile fracture. Twenty different specimens were tested per fibre type. Tungsten wire of standard size was used to measure the compliance of the system. The diameters of the individually tested filaments were measured using a 'Watson eyepiece' apparatus. The size and tensile properties of all the filaments are listed in *Table 1*.

RESULTS

Raman spectra

The Raman spectra of aramid and PBZT fibres within the frequency region of $1200–1700\,cm^{-1}$, have been shown in ref. 5 (Figures 4 and 5, p. 1790). The spectroscopic–mechanical studies in this work were performed by monitoring the deformation of a number of prominent vibrations of the polymer backbone (*Table 2*).

Compression loading

Typical cantilever compression plots are produced with the y-axis co-ordinate representing the Raman frequency difference — or shift — between the values obtained from the embedded fibre and the values of the corresponding stress-free fibre in air, and with the x-axis co-ordinate representing the compressive strain calculated point-by-point along the fibre length[5,20]. The Raman frequency

Table 1 Tensile properties of LCP fibres

Fibre	Diameter (μm)	Tangent Young's modulus at 1% strain (GPa)	Tensile fracture strain (%)	Tensile strength (MPa)
Kevlar 29	12.0	80±15	3.0±0.2	2400±250
Kevlar 49	12.0	120±10	2.5±0.2	3250±200
Kevlar 149	12.5	160±20	1.2±0.3	1920±250
Kevlar 49 (HT1420d)	11.9	125±10	2.5±0.2	3400±250
Kevlar 49 (HT2160d)	14.6	120±10	2.6±0.3	3600±300
PBZT	16.5	260±20	1.4±0.3	3920±300

Table 2 Spectroscopic data for LCP fibres

Fibre	Frequency (cm^{-1})	Assignment
Kevlar	1615	Ring C–C stretching
PBZT	1480	Heterocyclic ring C–C stretching

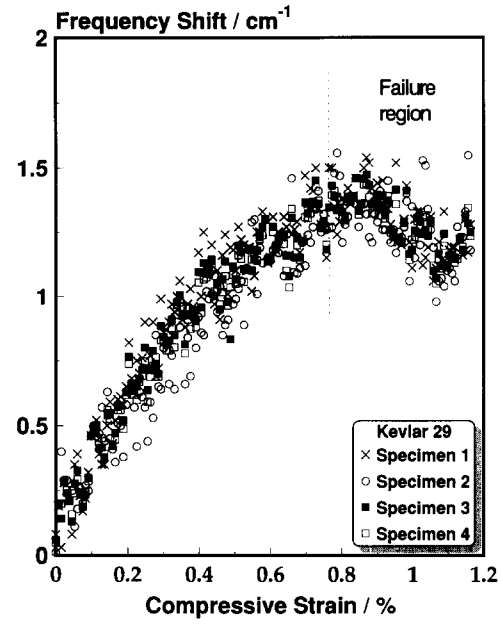

Figure 3 Raman frequency shift *versus* compressive strain for the Kevlar 29 fibre

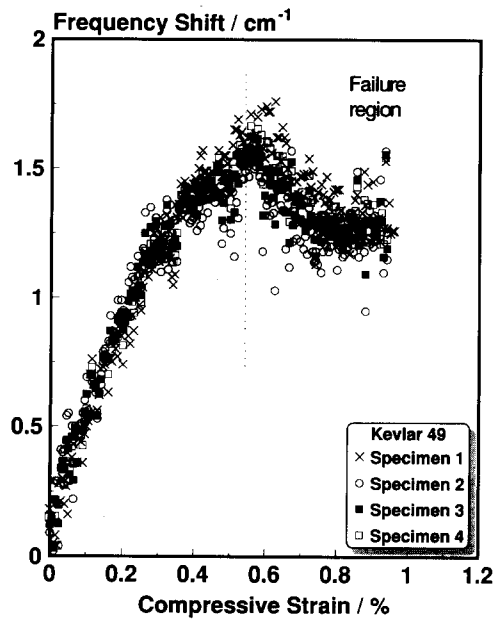

Figure 4 Raman frequency shift *versus* compressive strain for the Kevlar 49 fibre

versus compressive strain plots for Kevlar 29, 49, 49 HT1420d, 49 HT2160d, 149 and PBZT fibres, are shown in *Figures 3–8*. In the case of aramid fibres the Raman frequency increases with applied compressive strain up to a critical threshold value and then exhibits a somewhat sinusoidal fluctuation around a plateau value. The initial part of the loading curve prior to failure is distinctively non-linear particularly in the case of K29 (*Figure 3*) and K49 (*Figures 4–6*) fibres. The 'troughs' of the post-failure region correspond to areas of kink band formation as confirmed by simultaneous optical observations. On the contrary, the rigid-rod PBZT fibre (*Figure 8*) exhibits a more linear Raman frequency *versus* compressive strain behaviour prior to failure, which then forms a distinctive — albeit broad — plateau in the failure region.

For the Kevlar fibres, the higher the tensile modulus the lower the critical compressive strain which is required

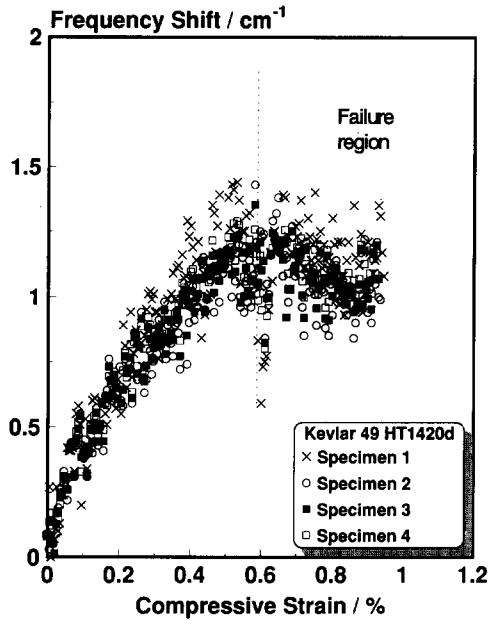

Figure 5 Raman frequency shift *versus* compressive strain for the Kevlar 49 HT1420d fibre

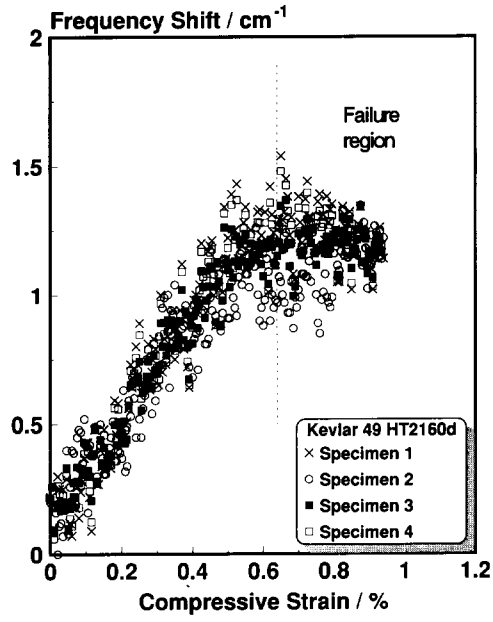

Figure 6 Raman frequency shift *versus* compressive strain for the Kevlar 49 HT2160d fibre

for the formation of the plateau (*Figures 3–7*). On the other hand, the stiffer rigid-rod PBZT fibre (*Figure 8*) 'yields' in compression at a strain value comparable to that of Kevlar 149 (*Figure 7*). No significant improvements in terms of critical compressive strain to failure were observed in the case of the heat-treated Kevlar 49 fibres (*Figures 5* and *6*). Finally, the difference in diameter in the case of the two Kevlar 49 heat-treated fibres (*Table 1*) does not seem to have a dramatic effect upon the critical compressive strain required for plateau formation (*Figures 5* and *6*).

Molecular deformation in tension and compression

As mentioned earlier, the cantilever beam can also be flexed in the opposite direction, hence subjecting the embedded fibre to a gradient of tensile load. Care has to be taken not to exceed the elastic limit of the cantilever beam itself therefore the fibres are normally loaded up to a maximum of 1–1.5% strain. By scanning along the fibre with the laser Raman probe, universal curves of Raman frequency *versus* applied strain can be produced in both tension and compression. Such curves are plotted in *Figures 9–14* for K29, 49, 49 HT1420d, 49 HT2120d, 149 and PBZT fibres, respectively. It can be clearly seen that all fibres remain intact up to 1% in tension but they 'yield' at relatively low values of applied strain in compression. In order to derive mathematical expressions for the Raman frequency *versus* (tensile or compressive) strain relationships, cubic spline interpolations are fitted to the raw data of *Figures 9–14*. The details of the fitting procedure are given in Appendix 2. It suffices to add here that in view of the abrupt changes of slope observed

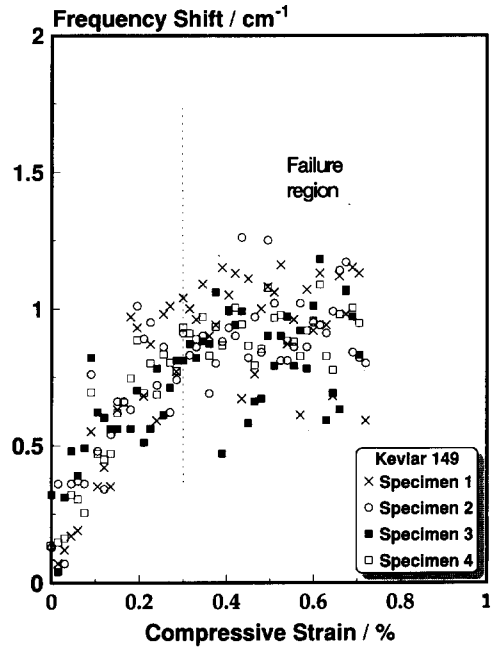

Figure 7 Raman frequency shift *versus* compressive strain for the Kevlar 149 fibre

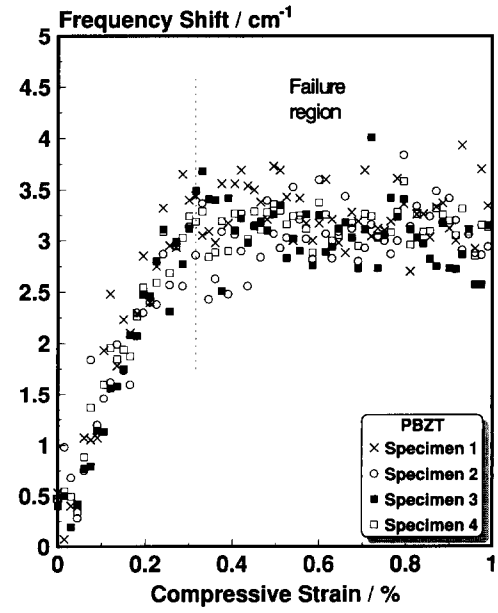

Figure 8 Raman frequency shift *versus* compressive strain for the PBZT fibre

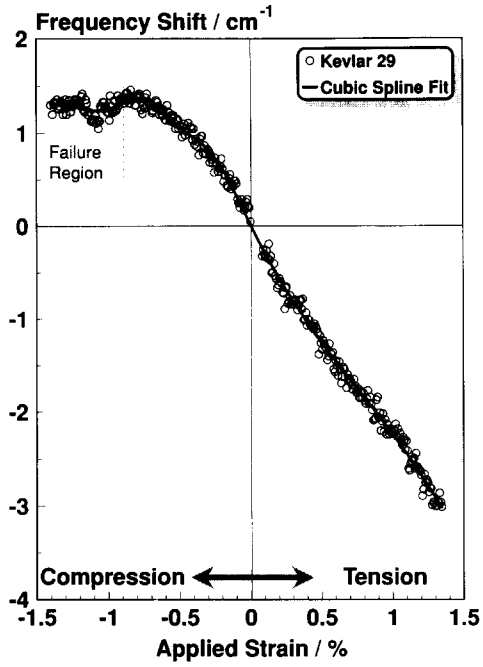

Figure 9 Raman frequency *versus* strain for the Kevlar 29 fibre within the range of −1.5 to 1.5% applied strain. Each data point represents an average of four measurements

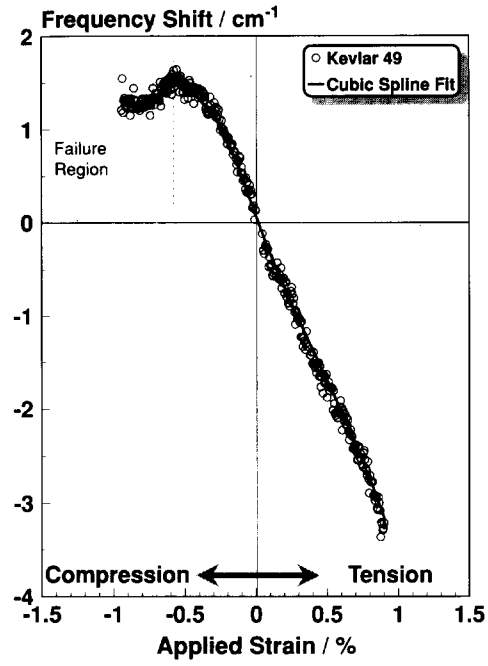

Figure 10 Raman frequency *versus* strain for the Kevlar 49 fibre within the range of −1.0 to 1.0% applied strain. Each data point represents an average of four measurements

during compression of LCP fibres, this is the only available method for obtaining representative fits to the experimental data across both tension and compression regimes. By contrast, any attempt to 'force' high-order polynomials[12] to the whole set of tension–compression data, leads to totally unsatisfactory fits to the experimental data (Appendix 2).

DISCUSSION

Modelling the deformation of polymer fibres

Several attempts have been made over the past 15 years to provide a description for the tensile deformation of LCP fibres such as Kevlar. Northolt[24] based his approach on the classical aggregate model[25] by considering the fibre as an aggregate of parallel arrays of identical fibrils consisting of crystallites arranged in series. For small deformations (<2%), the tensile strain, ε, in the fibre was estimated by Northolt and Hout[26] to be approximately equal to:

$$\varepsilon \cong \frac{\sigma}{e_c} + \frac{1}{2}\langle \sin^2 \theta_0 \rangle \left[1 - \exp\left(-\frac{\sigma}{g} \right) \right] \qquad (1)$$

where σ is the tensile stress applied along the fibre axis, e_c is the chain modulus, $\langle \sin^2 \theta_0 \rangle$ is an orientation

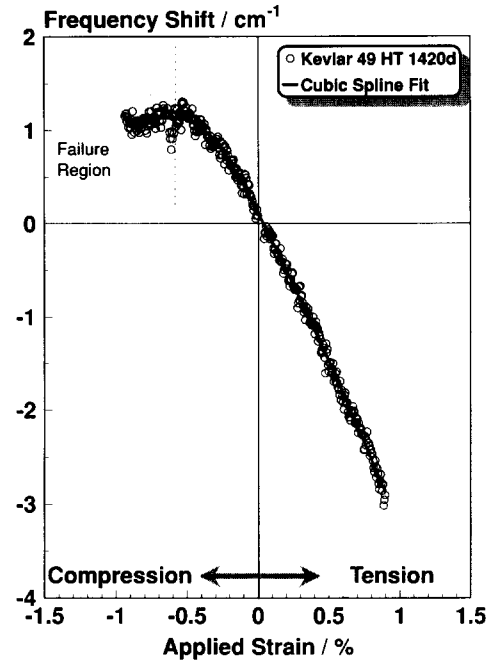

Figure 11 Raman frequency *versus* strain for the Kevlar 49 HT1420d fibre within the range of −1.0 to 1.0% applied strain. Each data point represents an average of four measurements

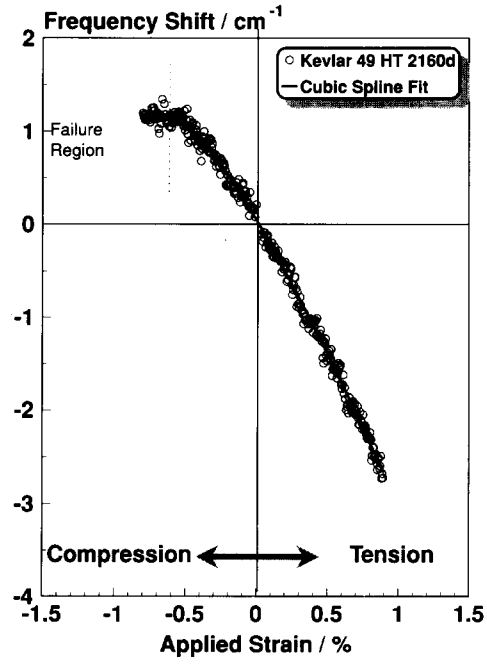

Figure 12 Raman frequency *versus* strain for the Kevlar 49 HT2160d fibre within the range of −1.0 to 1.0% applied strain. Each data point represents an average of four measurements

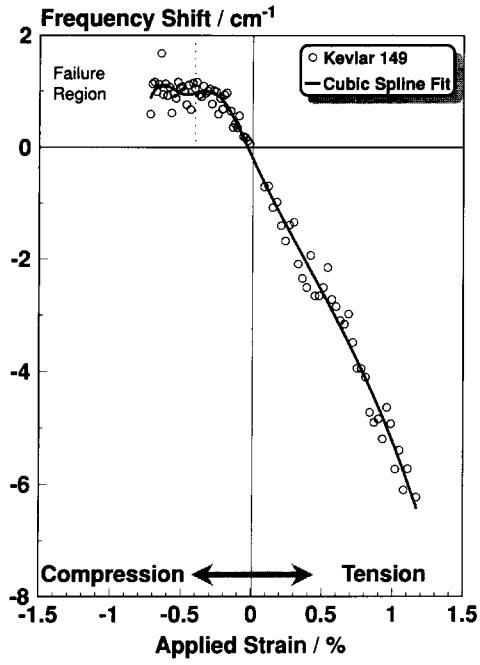

Figure 13 Raman frequency *versus* strain for the Kevlar 149 fibre within the range of −1.0 to 1.0% applied strain. Each data point represents an average of four measurements

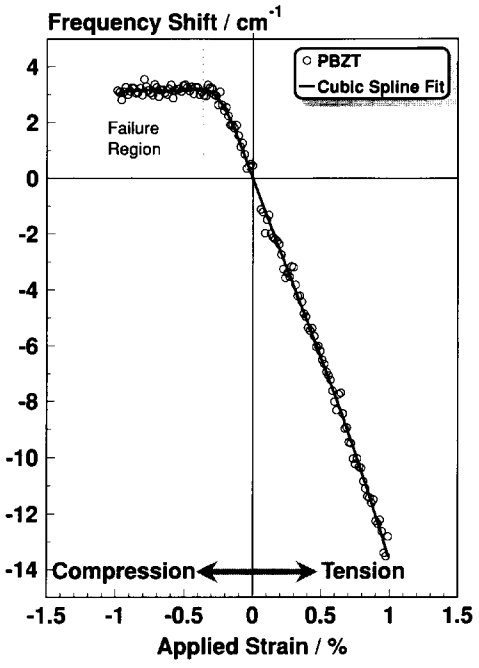

Figure 14 Raman frequency *versus* strain for the PBZT fibre within the range of −1.0 to 1.0% applied strain. Each data point represents an average of four measurements

parameter describing the average molecular orientation with respect to the filament axis and g is the shear modulus in the plane containing the symmetry axis of the crystallite.

An alternative 'macroscopic' approach proposed by Allen and Roche[27], departs from the classical aggregate model and attempts to model the deformation of Kevlar fibres as the progressive opening of the pleated structure which occurs via a local shear mechanism. It is indeed striking that by just considering the coupling between axial and shear stresses — as is normal practice in the field of composites loaded in a direction other than their principal axis — the following stress–strain equation can be derived for small deformations:

$$\varepsilon \cong \frac{\sigma}{e_s} + \frac{1}{2}(\tan^2\theta_0)\left[1-\exp\left(-\frac{2\sigma}{g}\right)\right] \quad (2)$$

where e_s here is the maximum stiffness of the fibre at high applied strains and θ_0 is the initial misorientation angle which for the pleated Kevlar 49 structure is estimated to be ~4–5°[27]. The parameters σ and g are the applied stress and shear modulus of the fibre as above.

The first term of equations (1) and (2) is the extensional strain component of the crystallites[26] or of the individual pleats[27] and the second term refers to the rotational strain towards the fibre axis due to shear deformation[26,27]. It is clear that in both approaches the total strain is the sum of the two deformation processes:

$$\varepsilon = \varepsilon_{\text{stretch}} + \varepsilon_{\text{rotation}} \quad (3)$$

Equations (1) and (2) are useful in that they predict the strain hardening effect observed during tensile loading of these fibres but fail to describe fully the dip in the tensile moduli data observed at 0.5% strain[27].

The shift of the Raman frequency, $\Delta\nu$, for a given backbone vibrational mode, is only due to the deformation of covalent bonds along the chain and is not affected by rotational or shearing motions[28]. For fibres, such as aramid or carbon[29], which can be considered as aggregates of crystallites connected in series, the $\Delta\nu$ scales with the applied stress:

$$|\Delta\nu| = k\sigma \quad (4)$$

where k represents the sensitivity of the Raman frequency shift to an applied stress. This is shown clearly in *Figure 15a* where a linear relationship of an average slope of $k = 4.0\,\text{cm}^{-1}\,\text{GPa}^{-1}$ is obtained out of five independent experiments on Kevlar 49 fibres. In fact, linear relationships of almost identical slopes have been obtained for a whole range of aramid fibres[30]. By differentiation, equation (4) becomes:

$$\mathrm{d}|\Delta\nu| = k\,\mathrm{d}\sigma \quad (5)$$

Furthermore by dividing both terms by the axial strain differential, $\mathrm{d}\varepsilon$, we obtain:

$$\frac{\mathrm{d}|\Delta\nu|}{\mathrm{d}\varepsilon} = k\frac{\mathrm{d}\sigma}{\mathrm{d}\varepsilon} = kE_{(\varepsilon)} \quad (6)$$

where $E_{(\varepsilon)}$ is the strain-dependent fibre tangent modulus. Equations (5) and (6) state that a family of LCP fibres (e.g. aramid) derived from the same precursor by hot-drawing, should have one value of k associated with them regardless of their respective (tangent) Young's moduli. In *Figure 15b*, the derivative of the Raman frequency shift with respect to strain at 0% strain (see Appendix 2), is plotted against the initial Young's modulus for the aramid fibres examined in this work. As found previously[28], a straight line can be fitted to the commercial Kevlar data and this again confirms the validity of equation (6). The value of k [equation (10)] can be taken as $3.8\,\text{cm}^{-1}\,\%^{-1}$ which is the slope of the least-squares-fitted line of *Figure 15b*. It is interesting to note that Du Pont's proprietary annealing process which affects drastically the structure of the fibres also affects the value of k (*Figure 15b*).

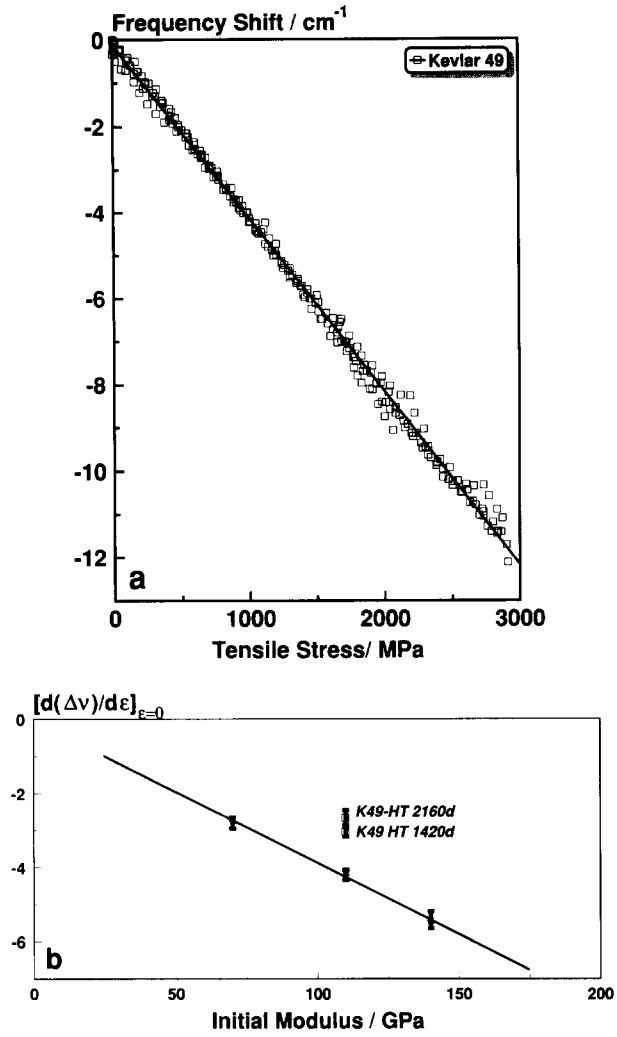

Figure 15 (a) Raman frequency shift *versus* applied stress for five different Kevlar 49 fibres. The slope of the least-squares-fitted line is $-4.0\,cm^{-1}\,GPa^{-1}$. (b) Rate of change of the Raman frequency shift at 0.0% strain as a function of the initial tangent Young's modulus for all aramid fibres tested in this work. The slope of the least-squares-fitted line is $-3.8\,cm^{-1}\,GPa^{-1}$

Strain dependence of axial modulus in tension and compression

As mentioned above, the Raman data in tension and compression of *Figures 9–14*, can be fitted well with spline polynomial regressions of the form:

$$\Delta\nu = f_0 + f_1\varepsilon + f_2\varepsilon^2 + \cdots \quad (7)$$

where $\Delta\nu$ is the Raman frequency shift and the f terms are the polynomial coefficients. The sensitivity of the Raman frequency, $\alpha_{(\varepsilon)}$, to an applied strain, can be represented by the first derivative of the above equation:

$$\alpha_{(\varepsilon)} = \frac{d|\Delta\nu|}{d\varepsilon} = f_1 + 2f_2\varepsilon + \cdots \quad (8)$$

As stated in equation (6), the parameter $\alpha_{(\varepsilon)}$ scales with the strain-dependent tangent modulus $E_{(\varepsilon)}$ of LCP fibres. Furthermore, $\alpha_{(\varepsilon)}$ can be defined at any level of fibre strain through the cubic spline polynomial regressions of equation (1) of *Figures 9–14*. Henceforth, tangent modulus *versus* strain curves can simply be obtained by dividing equation (8) by k [equation (6)]:

$$E_{(\varepsilon)} = \frac{\alpha_{(\varepsilon)}}{k} = \frac{f_1}{k} + 2\frac{f_2}{k}\varepsilon + \cdots \quad (9)$$

Alternatively, if k is not known, one can measure, for example, the initial tensile modulus of the fibres, E_0 and, therefore, an estimate of modulus $E_{(\varepsilon)}$ at any value of strain (compressive or tensile) can be obtained from the equation:

$$E_{(\varepsilon)} = E_0\frac{\alpha_{(\varepsilon)}}{\alpha_{(0)}} \quad (10)$$

where $\alpha_{(0)}$ is the first derivative of the Raman frequency shift *versus* strain data at 0% strain.

In *Figures 16*, *17* and *18*, the estimated modulus is plotted against the applied strain for the families of

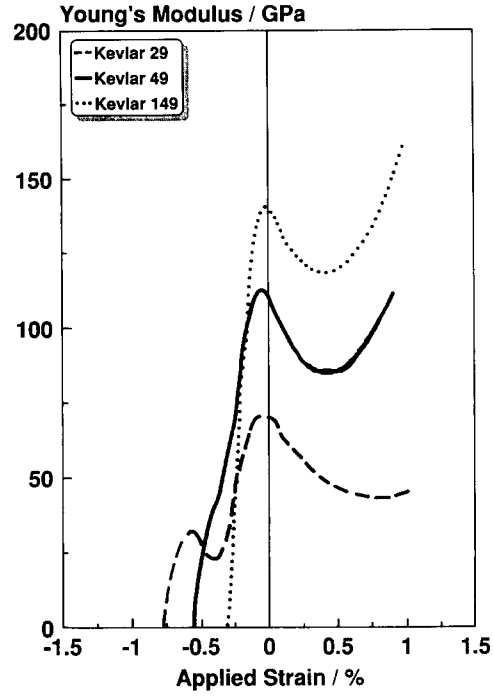

Figure 16 Estimated Young's modulus *versus* applied strain for the commercial Kevlar fibres

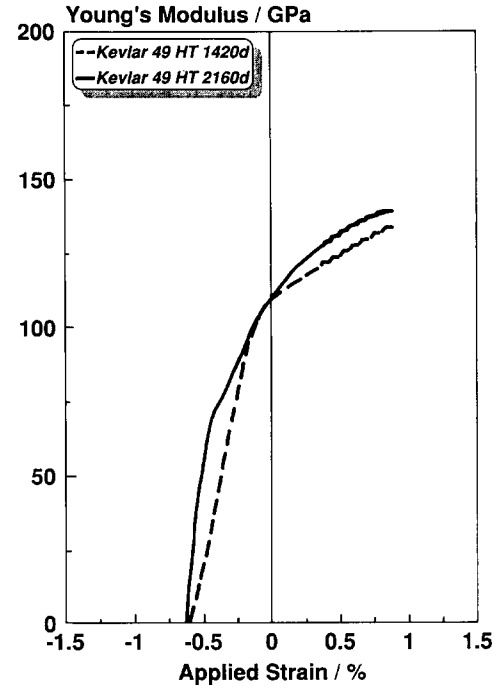

Figure 17 Estimated Young's modulus *versus* applied strain for the Kevlar HT1420d and HT2160d fibres

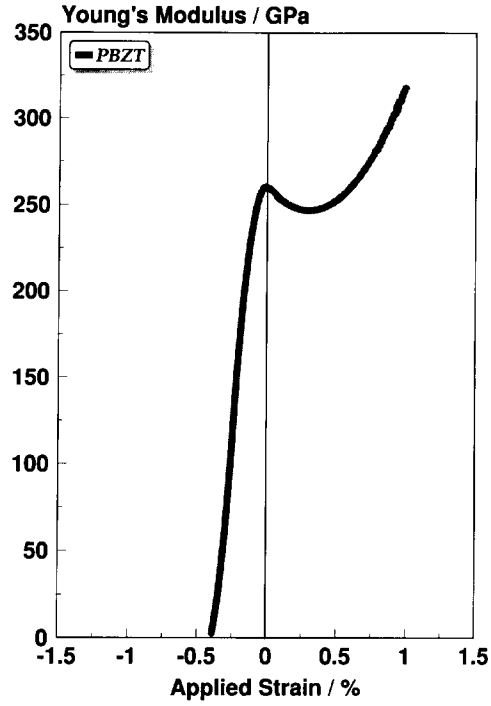

Figure 18 Estimated Young's modulus *versus* applied strain for the PBZT fibre

commercial Kevlar fibres, the heat-treated Kevlar and PBZT, respectively. In the case of the commercial Kevlar fibres (*Figure 16*), a dramatic drop of Young's modulus is observed in compression whereas a strain hardening effect is obtained at strains higher than ~0.5%. With the exception of Kevlar 149, the observed behaviour in tension looks strikingly similar to the mechanical results obtained by Allen and Roche[27]; an initial drop of modulus at ~0.05% of strain is followed by a modulus increase at higher strains. Indeed, if the fibre is regarded as a chain of crystallites, each having a slight misorientation with respect to the fibre axis, then the application of a tensile load will tend to align the crystallites to the loading direction[28], whereas, the application of compressive load will tend to align the crystallites normal to the loading direction[5]. Similarly, at the supramolecular level, this strain-hardening effect is thought to correspond to the opening-up of the 'pleated' structure in response to the tensile deformation at strains higher than 0.5% (fibre axis)[27]. By contrast, the 'heat-treated' Kevlar fibres (*Figure 17*), do not exhibit the initial drop of tensile modulus observed in the commercial Kevlar (*Figure 16*) and, furthermore, show a lower rate of modulus increase with strain. Finally, PBZT fibres (*Figure 18*) also exhibit pronounced strain-hardening in tension as a result of their microfibrillar texture[31].

LCP fibres generally possess a high degree of anisotropy and are extremely weak in the transverse direction. Therefore, when tested in compression, all individual LCP domains are expected to rotate to a direction normal to the loading direction (fibre axis) and this leads to a marked reduction of the compression modulus with applied strain. However, unlike loading in tension where strain hardening is only observed beyond a certain threshold limit of strain (0.5% for commercial Kevlars), the modulus in compression is reduced as soon as a compressive load is applied. Furthermore, in all cases examined here, the rate of strain-softening in compression exceeds by far the corresponding rate of strain-hardening in tension. This indicates that the LCP fibres are extremely unstable in compression with internal fibrils bending invariably out-of-plane as the load increases.

Stress–strain curves in tension and compression

By combining the stress-controlled [equation (4), *Figure 15a*] and the cantilever strain-controlled experiments [equation (7), *Figures 9–14*], an estimated stress–strain function in both tension and compression can be derived by:

$$\sigma = \frac{f_0}{k} + \frac{f_1}{k}\varepsilon + \frac{f_2}{k}\varepsilon^2 + \cdots \qquad (11)$$

where σ is the applied stress, ε the applied strain, f the coefficients of the spline polynomial and k the stress dependence of the Raman frequencies [equation (4), *Figure 15*]. In *Figures 19–21*, these spectroscopically derived stress–strain curves are shown. The corresponding values of compressive strength for each fibre are listed in *Table 3*.

The derived stress–strain curves display quite clearly all the prominent features of the macroscopic deformation of LCP fibres: exceptional strength and stiffness in tension and modulus softening followed by abrupt 'yielding' at low values of stress–strain, in compression. An inspection of the stress–strain curves for the commercial Kevlar fibres (*Figure 19*) reveals that the initial compression modulus follows the trend observed in tension, i.e. K149 > K49 > K29. However, in spite of their differences in terms of values of compression modulus, all fibres fail by kinking when a compressive stress of ~300 MPa is reached. The annealing process seems to alter the strain dependence of the macroscopic modulus (*Figure 17*) but affects only marginally the stress–strain behaviour in compression as shown in *Figure 20*. Finally, the rigid-rod PBZT fibre (*Figure 21*) exhibits a similar type of stress–strain behaviour to that of the aramid fibres with the whole curve 'pivoted' around the origin to higher values of stiffness.

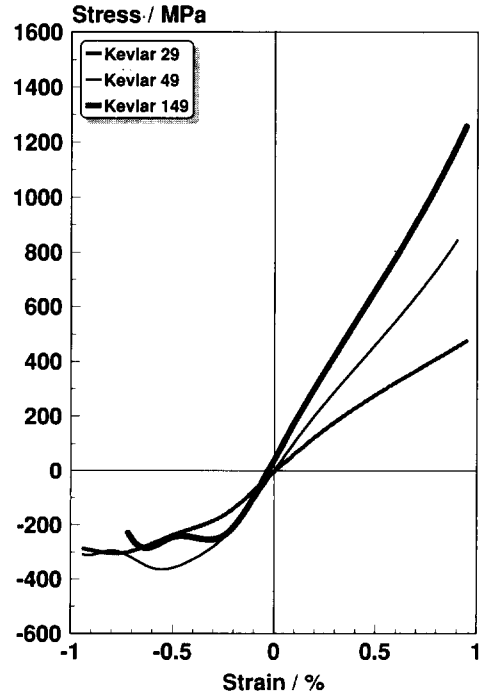

Figure 19 Stress–strain relationships in tension and compression for the commercial Kevlar fibres

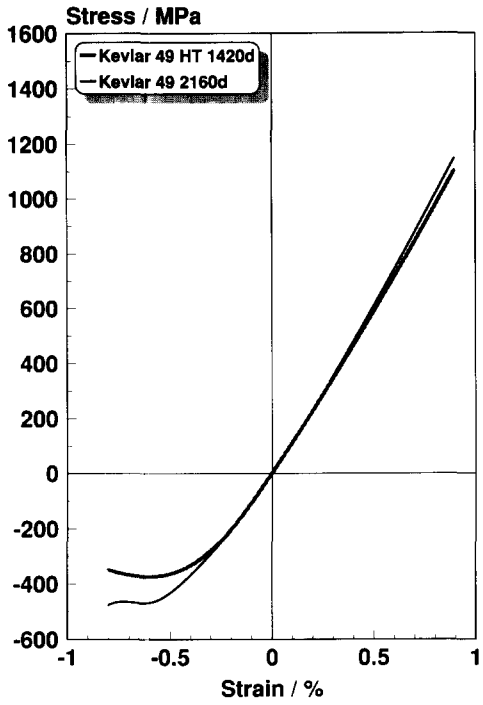

Figure 20 Stress–strain relationships in tension and compression for the Kevlar HT1420d and HT2160d fibres

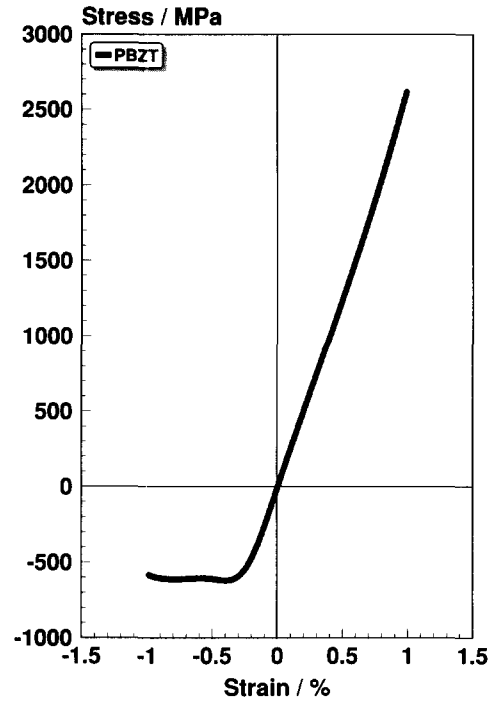

Figure 21 Stress–strain relationship in tension and compression for the PBZT fibre

Table 3 Compressive properties of LCP fibres

Fibre	Initial Young's modulus (GPa)	Compressive strain to failure (%)	Compressive strength (MPa)
Kevlar 29	70	0.75±0.05	304±45
Kevlar 49	110	0.55±0.05	362±40
Kevlar 149	140	0.30±0.10	260±60
Kevlar 49 HT1420d	110	0.60±0.05	373±30
Kevlar 49 HT2160d	110	0.60±0.05	469±30
PBZT	260	0.35±0.05	620±40

Estimates of compressive strength

In *Figure 22* the estimated values of maximum compressive stress are plotted as a function of the initial Young's modulus for all the fibres examined in this work. The actual values of compressive strength for each fibre are also listed in *Table 3*. As can be seen, all commercial aramid fibres fail within experimental error at a compressive stress of ~300 MPa. Du Pont's proprietary annealing process does not seem to improve drastically the compression behaviour of the 1420 denier fibre. On the other hand, a moderate increase in the compressive strength is observed in the case of the 2160 denier fibre. It is not, however, clear whether this improvement is due to a size effect or to changes in the morphology–structure of the fibre as a result of the annealing process.

The value of 620±40 MPa derived for the PBZT fibre is much higher than the value obtained in the first part of this series[5]. The reason for this discrepancy is that, previously (ref. 5, Figure 9), any deviation from linearity of the Raman frequency *versus* strain plot was considered as the onset of fibre failure. However, as demonstrated here, all LCP fibres exhibit gradual strain-softening in compression and therefore the correct 'failure criterion' should be defined as the strain (or stress) required for the compression tangent modulus to become zero (*Figure 18*). Optical observations of the locus of failure on the cantilever beam cannot provide accurate values of compressive strain to failure as the observed kinks or bulges always appear after the onset of failure (e.g. the 'troughs' in *Figures 3* and *4* correspond to kink bands).

Mechanisms of compression failure in LCP fibres

There are clear parallels between fibre kinking in compression and microbuckling in composites. Rosen[32] assumed that the microbuckling in composites is an elastic bending/buckling phenomenon and derived a formula relating the kinking stress σ_c to the shear modulus of the matrix, G_m:

$$\sigma_c = \frac{G_m}{1 - V_f} \tag{12}$$

where V_f is the fibre volume fraction. As pointed out elsewhere[33], equation (12) should be interpreted as $\sigma_c = G$, where G is the effective longitudinal shear modulus of the composite. Argon[34] considered the microbuckling phenomenon as a plastic shear instability and proposed the following formula for σ_c:

$$\sigma_c = \frac{\tau_y}{\phi} \tag{13}$$

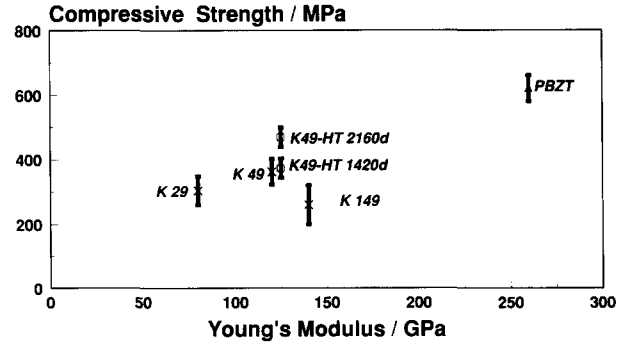

Figure 22 Estimated compressive strength as a function of the initial Young's modulus for the LCP fibres studied in this work

where τ_y is the composite yield stress in longitudinal shear and ϕ is the initial fibre misalignment. Finally, Budiansky[35] modified Argon's formula [equation (13)] for an elastic-perfectly plastic composite to:

$$\sigma_c = \frac{\tau_y}{\gamma_y + \phi} = \frac{G}{1 + \frac{\phi}{\gamma_y}} \tag{14}$$

where $\gamma_y = \tau_y/G$ is the yield strain in longitudinal shear. It is important to note that Budiansky's treatment yields Rosen's formula for $\phi = 0$ and is asymptotically equivalent to Argon's approach for large values of ϕ.

A theoretical analysis for the onset of kink formation in rigid or semi-rigid rod fibres in terms of an elastic buckling of the polymer macromolecule has been carried out by DeTeresa *et al.*[16,36]. Their approach is based entirely on Rosen's earlier work for composites[32] and it is not surprising that it predicts that $\sigma_c = G$, where G is now the longitudinal shear modulus of the fibre. Comparison of experimental and predicted values has shown[36] that this theory overestimates the compressive strength typically by a factor of 3–4. In fact, it is not coincidental that the Rosen analysis overpredicts[33] the compressive strength of composites also by a factor of ~4–5. These findings suggest that for commercial fibres and composites microbuckling is predominantly a plastic rather than an elastic event and therefore the Argon–Budiansky model [equation (14)] provides a more appropriate basis for analysis.

As argued above, the LCP fibres can be essentially modelled as aggregates of crystallites connected in series. The strain hardening in tension and the corresponding strain-softening in compression can be attributed to axial-shear coupling and associated orientation (or misorientation) of crystallites/pleats in Kevlars or fibrils in PBZT. Equally, it is reasonable to assume that the shear instability induced in compression by $\phi > 0$ or as suggested in reference 19 by an initial orientation distribution $\langle\phi\rangle$, will be the predominant mechanism of failure in compression.

In *Figure 23* the present σ_c data for commercial Kevlar fibres and PBZT, are plotted against G. The values of G for PBZT, K49 and K29 are taken from reference 36,

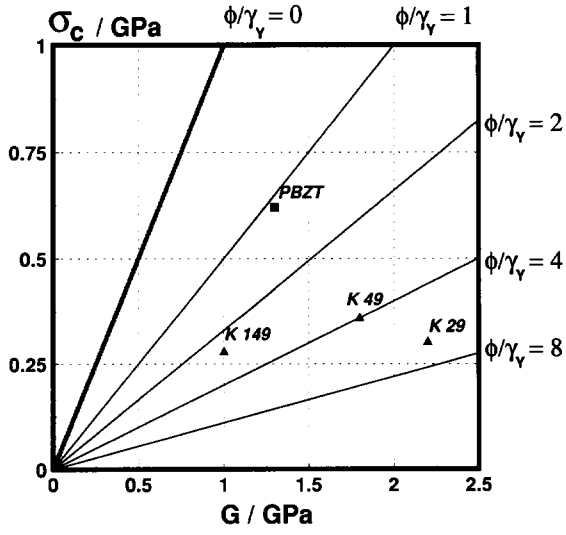

Figure 23 Compression 'yield' strength as a function of shear modulus for all the fibres tested in this work

whereas the value for K149 has been supplied by Allen[37]. For the PBZT fibre which exhibits a narrow distribution of orientation angles ϕ along the fibre direction, a good agreement is obtained for ϕ/γ_y of ~1. For the K29, K49 and K149 fibres the corresponding values of ϕ/γ_y are ~6, 4 and 3, respectively. By setting $\gamma_y = 0.02$ for the K49 fibre (onset of non-linear behaviour[38]), a misalignment angle ϕ of 4.5° is obtained which is in good agreement with previously reported values[27,39–41]. If we also assume a value of $\gamma_y = 0.02$ for K29 and K149 then angles of ~7° and 3° are obtained, respectively, which represent quite reasonable estimates for both fibres. It is concluded, therefore, that the inherent weakness of LCP fibres in compression, is a consequence of their instability in shear (low values of γ_y and G). Hence, any improvements in $\langle\phi\rangle$ brought about by means of hot-drawing, are bound to have very little effect upon σ_c [equation (14)].

One important issue which cannot be tackled by the 'macroscopic' approaches expressed by the models of equations (12)–(14), is the exact mode of failure at the molecular level. In tension, failure normally initiates by chain scission at a local stress concentration site and then propagates in the longitudinal direction. In compression, recent molecular dynamics calculations of 'rigid-rod' macromolecules such as PBZT[42], have shown that these molecules have an inherently 'soft' out-of-plane deformation mode even at room temperature and therefore viewed individually exhibit a pronounced sinusoidal trajectory. Furthermore, molecular orbital calculations[4] have shown that if a compressive load is imparted to a rigid-rod macromolecule like PBZT, the C–C bond, phenyl group and heterocyclic moiety are compressed initially, whereas the torsion angle increases twisting the two groups (*Figure 1*) out of planarity. It is worth adding here that the actual compression of the heterocyclic moiety has been experimentally confirmed by the shift of the corresponding Raman vibrational frequency to higher values with increasing compressive strain. When the input compressive energy reaches a threshold value, the molecule begins to bend out-of-plane[4] and the bond lengths cannot be further decreased as confirmed by laser Raman spectroscopy. Such a molecular 'kinking' occurring locally at low stresses may well trigger the corresponding microscopic kinking of the fibre. The fact that the typical dimensions of a kink in the direction of the fibre axis are smaller than the average length of a rigid-rod molecule[19] provides further evidence for the existence of a shear-instability phenomenon at a much smaller scale than ever envisaged before. Further discussion and analysis of these points will be presented in a future publication[43].

CONCLUSIONS

Various types of semi-rigid rod Kevlar 49 fibres and a rigid-rod PBZT fibre, have been subjected to tension and compression using identical experimental conditions. For the Kevlar fibres, the higher the tensile modulus the lower the critical compressive strain required for compression 'yielding'. On the other hand, the stiffer rigid-rod PBZT fibre 'yielded' in compression at a strain value comparable to that of Kevlar 149. No significant improvements in terms of critical compressive strain to failure were observed in the case of the heat-treated Kevlar 49 fibres. Furthermore, the differences in size of the two Kevlar 49

heat-treated fibres did not have a dramatic effect upon the critical compressive strain to failure.

Universal Raman frequency *versus* strain curves in tension and compression have been produced for all the fibres tested here. These curves have been converted into axial modulus *versus* strain curves in tension and compression. The basis for this conversion has been the scalingof $\Delta\nu$ with applied stress [equation (4)], which has been verified experimentally. In the case of all commercial Kevlar fibres, a dramatic drop of Young's modulus was observed in compression whereas a strain hardening effect was obtained at strains higher than $\sim 0.5\%$. The PBZT fibre also exhibited strain-hardening in tension and pronounced strain-softening in compression. By contrast, the heat-treated Kevlar fibres exhibited a lower rate of modulus increase with strain in tension and a pronounced strain-softening effect in compression.

By fitting cubic spline polynomials to the frequency *versus* strain data, stress–strain functions for all the fibres examined here could be derived via equation (11). For the commercial Kevlar fibres the initial compression modulus followed the trend observed in tension, i.e. K149 > K49 > K29. All commercial Kevlar fibres failed by kinking at a compressive stress of ~ 300 MPa. The annealing process altered the strain dependence of the macroscopic modulus but affected only marginally the stress–strain behaviour in compression. Finally, the rigid-rod PBZT fibre exhibited a similar type of stress–strain behaviour to that of the aramid fibres with the whole curve 'pivoting' around the origin to higher values of stiffness. A relatively high compressive strength value of 620 MPa was derived for the PBZT fibres of this work.

The current models of fibre/composite compression failure have been briefly reviewed in the light of the experimental results presented here. Evidence has been shown to suggest that the inherent weakness of LCP fibres in compression, is a consequence of their plastic instability in shear as manifested by their inherently low values of γ_y and G.

ACKNOWLEDGEMENTS

We would like to thank Professor E. H. Andrews, Dr E. Kellar, Dr N. Melanitis (QMW) and Dr S. R. Allen, Dr Y. Termonia (Du Pont), for useful comments during the preparation of this manuscript. One of us (CV) is grateful to the Pateras Foundation for a studentship. Mr V. Chohan is thanked for performing the Raman frequency *versus* stress experiments. E. I. du Pont de Nemours Co. (Wilmington, USA) and the Defence Research Agency (DRA-RAE) are thanked for supplying the fibres. Finally the financial support of the Department of Trade and Industry, the Defence Research Agency (DRA-RAE), the Science and Engineering Research Council, E. I. du Pont de Nemours (USA) and the Dow Chemicals Co. (Europe), is gratefully acknowledged.

REFERENCES

1 Yang, H. H. 'Aromatic High Strength Fibres', John Wiley & Sons, New York, 1989
2 Krause, S. J., Haddock, T. B., Vezie, D. L., Lenhert, P. G., Hwang, W.-F., Price, G. E., Helminiak, T. E., O'Brien, J. F. and Adams, W. W. *Polymer* 1988, **29**, 1354
3 Adams, W. W. and Eby, R. K. *Mater. Res. Soc. Bull.* 1987, **XII**, 22
4 Wierschke, S. G., Shoemaker, J. R., Haaland, P. D., Pachter, R. and Adams, W. W. *Polymer* 1992, **33**, 3357
5 Vlattas, C. and Galiotis, C. *Polymer* 1991, **32**, 1788
6 Sinclair, D. *J. Appl. Phys.* 1950, **21**, 380
7 Jones, W. R. and Johnson, J. W. *Carbon* 1971, **9**, 645
8 Greenwood, J. H. and Rose, P. G. *J. Mater. Sci.* 1974, **9**, 1809
9 Hawthorne, H. M. and Teghtsoonian, E. *J. Mater. Sci.* 1975, **10**, 41
10 Jahankhani, H. and Galiotis, C. in 'Interfaces in Polymer, Ceramic and Metal Matrix Composites' (Ed. H. Ishida), Elsevier, New York, 1988, p. 107
11 Van der Zwaag, S. and Kampschoer, G. in 'Integration of Fundamental Polymer Science and Technology' (Eds P. J. Lemstra and L. Kleintjens), 2nd Edn, Elsevier, Oxford, 1988, p. 545
12 Young, R. J. and Ang, P. P. *Polymer* 1992, **33**, 975
13 Allen, S. R. *J. Mater. Sci.* 1987, **22**, 853
14 Dobb, M. G., Johnson, D. J. and Park, C. R. *J. Mater. Sci.* 1990, **25**, 829
15 McGarry, F. J. and Moalli, J. E. *Polymer* 1991, **32**, 1811
16 DeTeresa, S. J., Porter, R. S. and Farris, R. J. *J. Mater. Sci.* 1988, **23**, 1886
17 Macturk, K. S., Eby, R. K. and Adams, W. W. *Polymer* 1991, **32**, 1782
18 Takahashi, T., Miura, M. and Sakuri, K. *J. Appl. Polym. Sci.* 1983, **28**, 579
19 Martin, D. C. and Thomas, E. L. *J. Mater. Sci.* 1991, **26**, 5171
20 Melanitis, N. and Galiotis, C. *J. Mater. Sci.* 1990, **25**, 5081
21 Timoshenko, S. P. and Gere, J. M. 'Theory of Elastic Stability', McGraw-Hill, New York, 1961
22 Galiotis, C. *Comp. Sci. Technol.* 1991, **42**, 125
23 ASTM D3379-75 (reapproved 1982). 'Standard Test Method for Tensile Strength and Young's Modulus for High Modulus Single Filament Materials'
24 Northolt, M. G. *Polymer* 1980, **21**, 1199
25 Ward, I. M. *Proc. Phys. Soc.* 1962, **80**, 1176
26 Northolt, M. G. and v. d. Hout, R. *Polymer* 1985, **26**, 310
27 Allen, S. R. and Roche, E. J. *Polymer* 1989, **30**, 996
28 Van der Zwaag, S., Northolt, M. G., Young, R. J., Robinson, I. M., Galiotis, C. and Batchelder, D. N. *Polym. Commun.* 1987, **28**, 276
29 Melanitis, N., Tetlow, P. L., Galiotis, C. and Smith, S. S. *J. Mater. Sci.* 1994, **29**, 786
30 Galiotis, C., Chohan, V., Wall, A. and Vlattas, C. to be published
31 Jiang, H., Eby, R. K., Adams, W. W. and Lenhert, G. *Mater. Res. Soc. Symp. Proc.* 1989, **134**, 341
32 Rosen, B. W. 'Mechanics of Composite Strengthening', ASM Seminar, American Society of Metals, Philadelphia, 1964
33 Budiansky, B. and Fleck, N. A. *J. Mech. Phys. Solids* 1993, **41**, 183
34 Argon, A. S. 'Treatise of Materials Science and Technology', Vol. 1, Academic Press, New York, 1972
35 Budiansky, B. *Comp. Struct.* 1983, **16**, 3
36 DeTeresa, S. J., Porter, R. S. and Farris, R. J. *J. Mater. Sci.* 1985, **20**, 1645
37 Allen, S. R. personal communication, 1993 (The K149 fibres tested by Allen were inherently split and the value of $G = 1$ GPa is an approximation for perfectly cylindrical fibres)
38 Knoff, W. F. *J. Mater. Sci. Lett.* 1987, **6**, 1392
39 Ballou, J. W. *Polym. Prepr.* 1976, **17**, 75
40 Dobb, M. G., Johnson, D. J. and Saville, B. P. *J. Polym. Sci., Polym. Phys. Edn* 1977, **15**, 2201
41 Panar, M., Avakian, P., Blume, R. C., Gardner, K. H., Gierke, T. D. and Yang, H. H. *J. Polym. Sci., Polym. Phys. Edn* 1983, **21**, 1955
42 Farmer, B. L., Chapman, B. R., Dudis, D. S. and Adams, W. W. *Polymer* 1993, **34**, 1588
43 Vlattas, C. and Galiotis, C. to be published
44 Hayes, J. G. *Bull. Inst. Maths Applics* 1974, **10**, 144

APPENDIX 1

Four-point bending beam method

A modified version of the cantilever bending beam (CB) was employed to study the compressional behaviour of LCP fibres in this paper. A four-point beam (FB) configuration has also been employed to verify the results obtained from CB tests. The beam in the latter case (*Figure A1a*) is supported by two fixed rollers whereas the two inner rollers can be moved up or down,

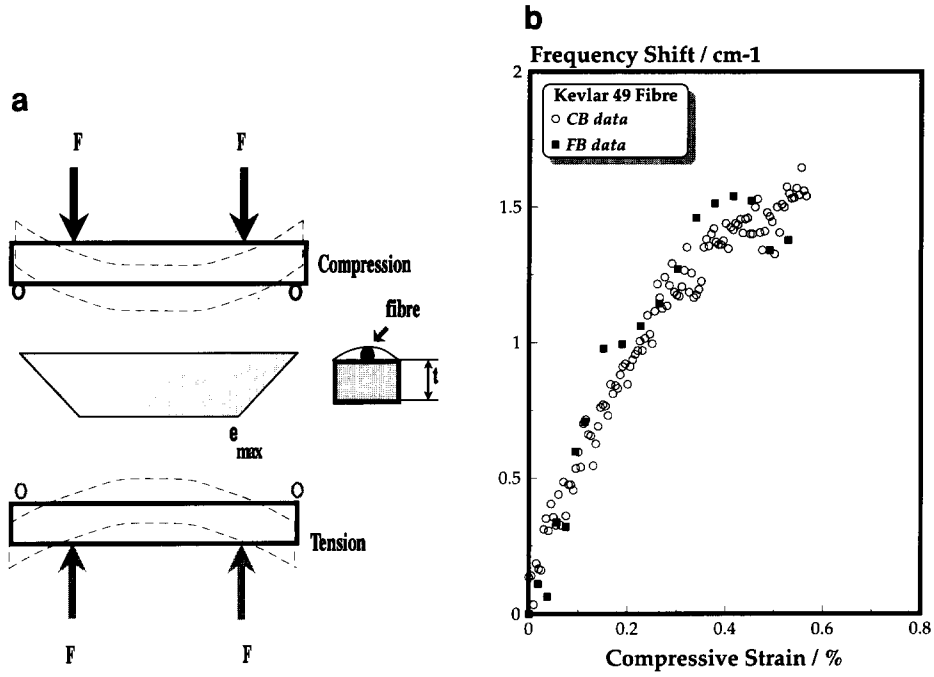

Figure A1 (a) Schematic representation of the four-point beam configuration. The e_{max} denotes the maximum strain of the surface of the beam between the inner loading points. (b) Raman frequency shift as a function of compressive strain for Kevlar 49 obtained using the cantilever beam (CB) and the four-point bend (FB) configurations. Each data point of CB represents an average of four measurements. Each data point of FB represents an average of four different measurements between the inner loading points and out of four different fibres

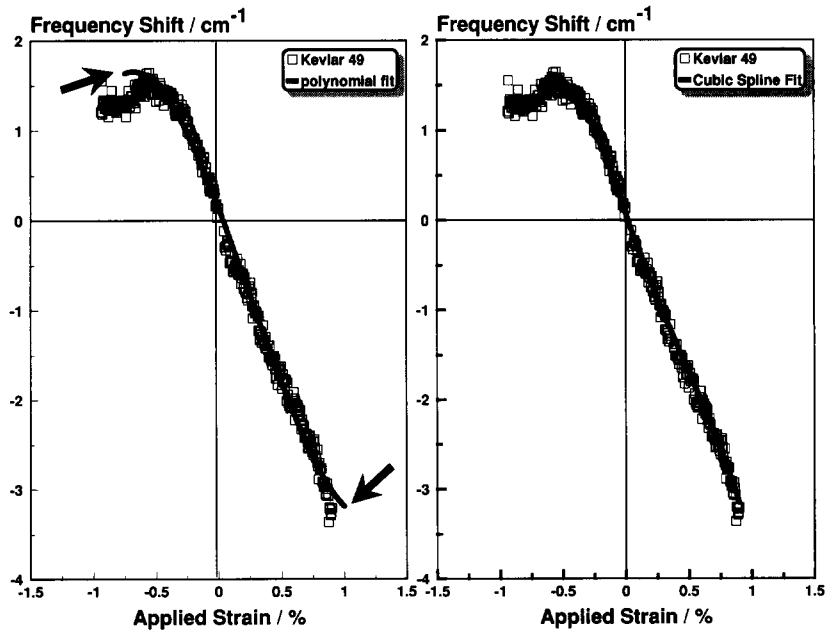

Figure A2 Raman frequency *versus* strain for the Kevlar 49 fibre within the range of −1.5 to 1.5% applied strain. The data have been fitted with third degree polynomial (left) and cubic spline (right) interpolations. The arrows indicate areas of poor fit in the case of the polynomial interpolation

subjecting the top surface of the beam between them to a uniform tensile or compressive strain.

The specimen preparation and testing was identical to the one employed in the CB method. A very sensitive strain gauge is glued on the top surface of the beam for instant reading of the strain field applied to the embedded fibres. The calibration curve for monitoring the strain on the fibre encapsulated in the thin acrylic film is obtained by testing dummy specimens (specimens with no fibre on their top surface). The indication of the strain gauge (i.e. resistance ΔR which is proportional to strain ε) is plotted as a function of the maximum deflection. Specimens are then positioned on the experimental stage and deflected stepwise into compression. Raman spectra between the inner loading points along the filaments are obtained before the next increase of strain.

The results obtained from the FB loading configuration for the Kevlar 49 fibre are compared with those obtained from CB in *Figure A1b*. As can be seen, the frequency *versus* compressive strain data for both CB and FB

geometries, are comparable within the experimental error. This indicates that the non-linearity of the Raman frequency *versus* compressive strain cannot be attributed to slippage between the fibre and the beam but it is an inherent property of the LCP fibres examined in this work.

APPENDIX 2

Cubic spline fitting to experimental data

In general, a set of data points which represent experimental measurements, contains random errors. To seek a functional approximation to the data, it is first necessary to specify the mathematical form of the function. The two basic requirements for approximating experimental data are smoothness and closeness. In the case of a polynomial fit the conflict of those two requirements is quite evident. Keeping the degree of the polynomial in fairly low level, smoothness can be achieved but the fit may be poor (little closeness). On the other hand, if the degree of the polynomial is too high, the fit will be too close to the data, essentially following the random errors and tending to have unwanted fluctuations between the data points.

In our case a cubic spline[44] was chosen as the fitting function to the Raman frequency *versus* strain data. It consists of a number of cubic polynomial segments joined end to end with continuity in first and second derivatives at the joints. The third derivative at the joints is in general discontinuous. The x-values of the joins are called knots, or more precisely, interior knots. Their number determines the number of coefficients in the spline, just as the degree determines the number of coefficients in a polynomial[44]. The choice of these knots is a matter of trial and error, though with a little experience a satisfactory choice can often be made after one or two trials. The following procedure was followed to fit the Raman frequency shift *versus* strain data:

- The knots were placed at equal distances of $\Delta x = 0.20$–0.25 in compression in order to fit accurately the abrupt changes of slope
- No knots were placed in tension since the slope change in this area was not as dramatic due to the fact that fibre failure did not occur within the 0–1.0% strain range (*Figures 9–14*).

In *Figure A2* the same set of experimental data has been fitted with the two different numerical methods, namely the polynomial and the cubic spline interpolations. As shown, the cubic spline interpolation gives a much more satisfactory fit to the experimental data. The polynomial fit is particularly poor in the area of compression failure where abrupt changes of Raman frequency *versus* strain slope occur.